Heterogeneity of HCN Half-Maximal Activation Potentials Can Explain Variability in Intrinsic Adaptation of Spiral Ganglion Neurons

Jason Boulet[1,2] and Ian Bruce[1,2,3]

[1]Auditory Engineering Laboratory, [2]McMaster Integrative Neuroscience Discovery & Study,
[3]Department of Electrical & Computer Engineering, McMaster University, Hamilton, ON, Canada

Abstract

Background It remains unclear as to why high-rate stimulation leads to variable outcomes of speech perception performance for people with cochlear implants (CIs). Although many factors might contribute to this perceptual variability, temporal interactions in the responses of spiral ganglion neurons (SGNs) likely contribute to variable constraints on acoustic information coding by CIs. Specifically, in response to high-rate electrical pulse train stimulation, electrical recordings of Type I SGNs have shown a large range in the degree to which they exhibit both subthreshold and spike-dependent adaptation of their excitability. A computational model by Negm and Bruce (2014) demonstrated that hyperpolarization-activated cyclic nucleotide-gated cation (HCN) channels may play an important role in regulating the degree of adaptation in response to pulse train stimulation. We hypothesize that experimentally observed heterogeneity in HCN half-maximal activation potentials could contribute to variability in adaptation.

Methods We developed a stochastic computational membrane model of cat Type I SGN based on the Hodgkin–Huxley (HH) model plus HCN and low-threshold potassium (KLT) conductances. We compared the simulation results obtained with the older HCN channel model taken from VCN cells (Rothman and Manis, 2003a) to those produced by a newer HCN model from SGNs (Liu et al., 2014). HCN half-activation potentials were explored over a physiologically-plausible range of values. Various stimulus paradigms were implemented to provide predictions of published in vivo CI stimulation data, including build-up and recovery of adaptation (Miller et al., 2011; Zhang et al., 2007) and refractory functions (Miller et al., 2001).

Results The simulation results showed that changing the half-activation potential of either type of HCN model could greatly influence the strength of adaptation that a model SGN exhibited to pulse-train stimuli, from strongly-adapting to non-adapting. Overall, the published data was best explained by the newer HCN channel model combined with the KLT channel model. Model absolute refractory periods were also observed to be within the known physiological range, in contrast to the Miller et al. (2011) adaptation model.

Conclusions Our results suggest that physiologically-realistic variation of HCN half-maximal activation potentials could determine the range of adaptation and recovery from adaptation seen in the physiological data while maintaining refractoriness within physiological bounds. [The authors would like to thank Dr. Paul Manis for supplying his HCN(*q*,*s*) channel model code and Dr. Paul Abbas for permitting use of previously published figures. Supported by NSERC Discovery Grant 261736.].

I. INTRODUCTION

- Studies such as the work by Arora et al. (2009) have demonstrated that speech perception is not necessarily improved by increasing the stimulation rate above 900 pulses/s per electrode. Adaptation may be partially responsible for the variability in speech perception by diminishing the SGN response for high-rate stimulation.
- Adaptation typically occurs on the order of 10 to 100 ms or more and is prevalent in SGN in response to a wide range of stimulation pulse rates and current levels (Heffer et al., 2010; Litvak et al., 2003; Miller et al., 2011; Zhang et al., 2007).
- Woo et al. (2009a,b, 2010) proposed a Hodgkin–Huxley model augmented with a spike-dependent extracellular potassium accumulation mechanism to explain spike rate adaptation. This was extended by Miller et al. (2011) to explain accommodation (subthreshold adaptation) by including KLT channels, but lead to unrealistic absolute refractory periods (ARPs).
- An alternative model proposed by Negm and Bruce (2014) was capable of producing spike rate adaptation and accommodation while also generating accurate ARP values. They used a HH model with extra HCN channels (Hugenard and McCormick, 1992; Rothman and Manis, 2003b) and KLT channels with activation and partial inactivation particles (Rothman and Manis, 2003a).
- The half-maximal activation potential ($V_{1/2}$) of HCN channels has known heterogeneity (–122 to –78 mV) across a range of several species, experimental preparations, developmental stages, and cochleotopy (Chen, 1997; Kim and Holt, 2013; Liu et al., 2014; Mo and Davis, 1997; Yi et al., 2010).
- We sought to test the hypothesis that varying the half-maximal activation potential of the old HCN model taken from murine VCN (Rothman and Manis, 2003b) or a newer HCN model obtained from basal SGN (Liu et al., 2014) could impact the strength of spike rate adaptation and accommodation in a membrane model of Type I SGN.

II. METHODS: Channel and Membrane Models

HCN Activation Functions and Time Constants

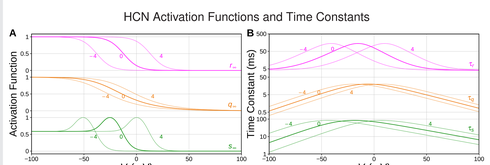

Figure 1: **A** Activation functions and **B** time constants for the HCN(r) (Rothman and Manis, 2003a) and HCN(q,s) (Liu et al., 2014) channel models as a function of the relative membrane potential V. Numbers shown beside the curves indicate how many $V_{1/2}$ standard deviations the functions have been shifted by (c).

HCN(r) Channel

$$i_{h,r}(t) = \gamma_h N_{h,r}(t)\,[V_m(t) - E_{h,r}]$$

$$r_0 \underset{\beta_r}{\overset{\alpha_r}{\rightleftharpoons}} r_1$$

HCN(q,s) Channel

$$i_{h,(q,s)}(t) = \gamma_h [N_{hq}(t) + N_{hs}(t)]\,[V_m(t) - E_{h,(q,s)}]$$

$$q_0 \underset{2\beta_q}{\overset{2\alpha_q}{\rightleftharpoons}} q_1 \underset{3\beta_q}{\overset{\alpha_q}{\rightleftharpoons}} q_2$$

$$s_0 \underset{\beta_s}{\overset{\alpha_s}{\rightleftharpoons}} s_1$$

Transition Rates

$$\alpha_x(V) = x_\infty(V)/\tau_x(V)$$

$$\beta_x(V) = [1 - x_\infty(V)]/\tau_x(V)$$

SGN Membrane Circuit Model

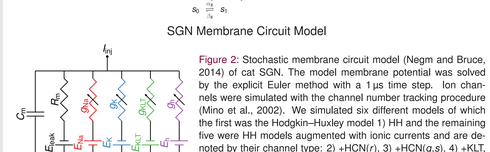

Figure 2: Stochastic membrane circuit model (Negm and Bruce, 2014) of cat SGN. The model membrane potential was solved by the explicit Euler method with a 1 µs time step. Ion channels were simulated with the channel number tracking procedure (Mino et al., 2002). We simulated six different models of which the first was the Hodgkin–Huxley model 1) HH and the remaining five were HH models augmented with ionic currents and are denoted by their channel type: 2) +HCN(r), 3) +HCN(q,s), 4) +KLT, 5) +HCN(r)+KLT, and 6) +HCN(q,s)+KLT.

III. RESULTS: What's In a Spike? Single Pulse Statistics

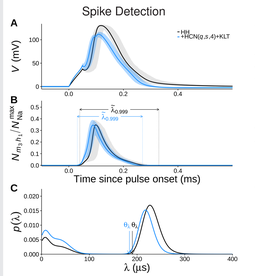

Figure 3: Determination of a spiking threshold based on the sodium conductance duration λ. Data from panels **A** and **B** represent 1000 independent responses to a 50 µs monophasic single pulse delivered at a current level equivalent to a FE of 99.9 %. **A** Relative membrane potential (V). **B** Proportion of open sodium ion channels ($N_{m_3h_1}/N_{Na}^{max}$). $\bar{\lambda}_{0.999}$ denotes the median sodium conductance duration, or the median duration over which $N_{m_3h_1}/N_{Na}^{max} > 0$ given a stimulus FE of 99.9 %. **C** Empirical probability density of λ marginalized over all stimulus current levels. The threshold θ_1 is said to be the minimum value of λ required to generate an action potential.

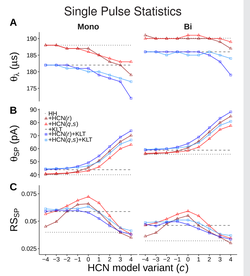

Figure 4: Monophasic and biphasic single pulse **A** sodium conductance duration threshold (θ_λ), **B** AP threshold current (θ_{SP}), and **C** relative spread ($RS_{SP} = \sigma_{SP}/\theta_{SP}$) as a function of the HCN $V_{1/2}$ shift parameter c. θ_{SP} and RS_{SP} were obtained by fitting the occurrence of spikes for 1000 trails over a range of current pulse amplitudes (I_{inj}) with 50 µs duration to

$$\mathrm{FE}(I_{inj}) = \frac{1}{2}\left[\mathrm{erf}\left(\frac{I_{inj} - \theta}{\sqrt{2}\sigma}\right) + 1\right].$$

III. RESULTS: Pulse Train Response

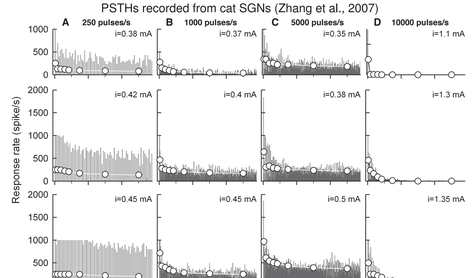

Figure 5: Cat SGN response rate as a function of the time since pulse train onset over a 300 ms interval. Subpanels with columnar arrangement indicate responses to stimulation at the rates of **A** 250 pulses/s, **B** 1000 pulses/s, **C** 5000 pulses/s, and **D** 10 000 pulses/s. Row-wise layout of the subpanels show an increasing biphasic pulse current level starting from the top panel to the bottom panel. Responses in panels **A**, **B**, and **C** were taken from a different SGN than those in panel **D**. Bars represent the response rate over 1 ms intervals and dots show the response rate over the progressively wider intervals (0–4, 4–12, 12–24, 24–36, 36–48, 48–100, 100–200, and 200–300 ms). This figure was adapted with kind permission of Springer Science & Business Media: Fig. 2 from Zhang et al. (2007), © 2007.

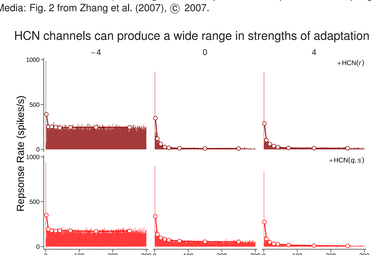

Figure 6: PSTH responses to pulse train stimulation over a 300 ms interval at a first-pulse FE of 80 % and rate of 2000 pulses/s for models +HCN(r) and +HCN(q,s) showing various strengths of adaptation as a function of the HCN $V_{1/2}$ shift parameter c. Bars and dots represent the same intervals as in Fig. 5. For all pulse train and masker-probe train stimulation, pulses were defined as 50 µs biphasic pulses with no interphase gap.

III. RESULTS: Pulse Train Response (cont'd)

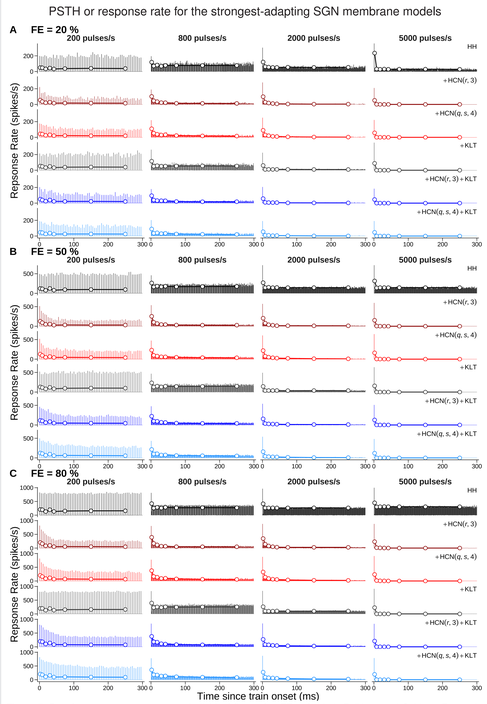

Figure 7: Panels represent responses to individual first-pulse FEs: **A** 20 %, **B** 50 %, and **C** 80 %. Row subpanels indicate membrane model and column subpanels represent stimulation rate. Bars and dots represent the same intervals as in Figs. 5 and 6.

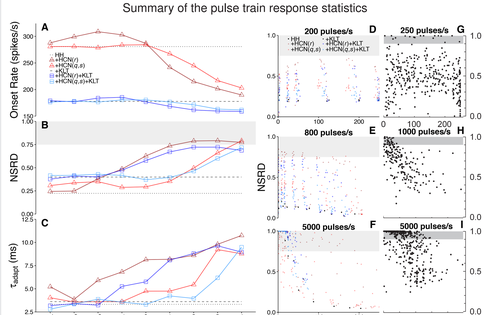

Figure 8: Pulse train responses for all SGN model variants given by **A** onset rate, **B** NSRD, and **C** τ_{adapt}, as a function of the HCN $V_{1/2}$ shift parameter c. τ_{adapt} was estimated from fitting the wide bin response rate data to $s(t) = A_{ss} + A_{asc}\exp(-t/\tau_{adapt})$. Simulation results shown in panels **A**, **B**, and **C** were averaged over all FEs (1, 10, 20, 50, 80, 99, 99.99, and 99.9999 %) and all pulse rates (200, 800, 2000, and 5000 pulses/s). SGN model simulation results for NSRD as a function of the onset response rate in response to pulse train stimulation at the **D** 200 pulses/s, **E** 800 pulses/s, and **F** 5000 pulses/s rates. Panels **D**, **E**, and **F** contain simulation results across all HCN $V_{1/2}$ levels (–4 to 4) and FEs (1, 10, 20, 50, 80, 99, 99.99, and 99.9999 %). The remaining panels correspond to the same NSRD versus onset response rate simulation plots, but for cat SGN recordings (Zhang et al., 2007) responding to **G** 250 pulses/s, **H** 1000 pulses/s, and **I** 5000 pulses/s pulse train stimulation. Note that the span of the onset response rate in panels **D** and **G** is 0 to 250 spikes/s whereas in panels **E**, **F**, **H**, and **I** it is 0 to 1000 spikes/s. Panels **G**, **H**, and **I** were adapted with kind permission of Springer Science & Business Media: Fig. 5, panels **B**, **E**, and **G** from Zhang et al. (2007), © 2007.

III. RESULTS: Probe Train Recovery Response

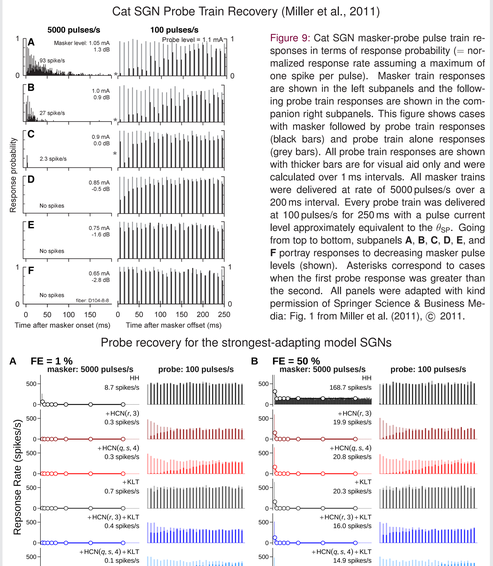

Figure 9: Cat SGN masker-probe pulse train responses in terms of response probability (= normalized response rate assuming a maximum of one spike per pulse). Masker train responses are shown in the left subpanels and the following probe train responses are shown in the companion right subpanels. This figure shows cases with masker followed by probe train responses (black bars) and probe train alone responses (grey bars). All probe train responses are shown with thicker bars are for visual aid only and were calculated over 1 ms intervals. All masker trains were delivered at rate of 5000 pulses/s over a 200 ms interval. Every probe train was delivered at 100 pulses/s for 250 ms with a pulse current level approximately equivalent to the θ_{SP}. Going from top to bottom, subpanels **A**, **B**, **C**, **D**, **E**, and **F** portray responses to decreasing masker pulse levels (shown). Asterisks correspond to cases when the first probe response was greater than the second. All panels were adapted with kind permission of Springer Science & Business Media: Fig. 1 from Miller et al. (2011), © 2011.

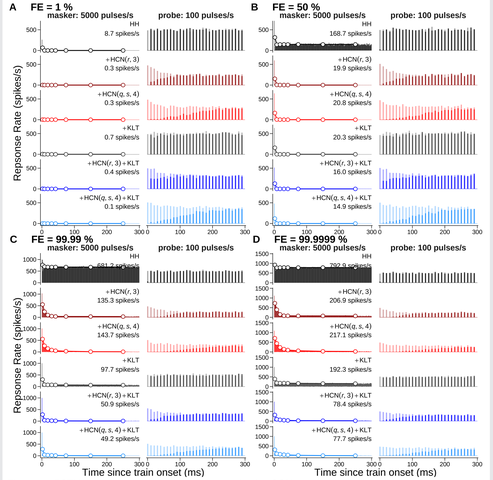

Figure 10: PSTH or response rate for the strongest-adapting SGN membrane models simulated over a 300 ms interval in response to a 5000 pulses/s masker train followed immediately by a 100 pulses/s probe train. Dark-colored bars represent responses to the condition with a masker train (masker-probe), whereas lighter-colored bars indicate that no masker train stimulated the neuron (probe-alone).

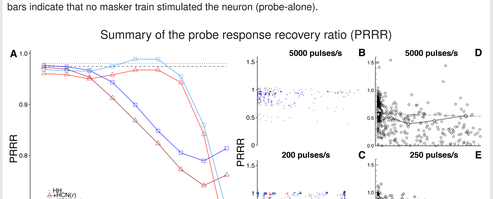

Figure 11: SGN model simulation results show the effect of **A** the HCN $V_{1/2}$ shift parameter c on the PRRR. Simulation results in panel **A** were averaged over all FEs and stimulation rates. SGN model simulation results for PRRR as a function of the mean response rate to the masker for the masker pulse train rates of **B** 5000 pulses/s and **C** 200 pulses/s. Panels **B** and **C** contain simulation results across all HCN $V_{1/2}$ levels (–4 to 4) and all FEs. Cat SGN recordings responding to **D** 5000 pulses/s and **E** 250 pulses/s masker-probe pulse train stimulation, where the mean response rate to the masker was calculated over the entire 0–200 ms masker train interval. Panels **D** and **E** were adapted with kind permission of Springer Science & Business Media: Fig. 3, panels **D** and **E** from Miller et al. (2011), © 2011.

III. RESULTS: Refractoriness

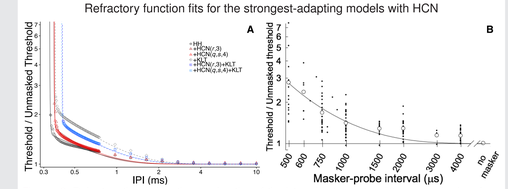

Figure 12: Refractory threshold ratio as a function of the interval between two 50 µs monophasic pulses. **A** Threshold / unmasked threshold (θ_{ref}/θ_{SP}) vs. interpulse interval (IPI) for the strongest-adapting SGN membrane models. Note that θ_{ref}/θ_{SP} and IPI are scaled on a log-10 axis. **B** Threshold / unmasked threshold as a function of the masker-probe interval (or IPI) from cat SGN (Miller et al., 2001). Panel **B** reprinted with kind permission of Springer Science & Business Media: Fig. 7 from Miller et al. (2001), © 2001. Data in panel **A** were fit to

$$\frac{\theta_{ref}}{\theta_{SP}} = \frac{\sum_{i=1}^{2} A_i}{\sum_{i=1}^{2} A_i\left[1 - \exp\left(-\left(\mathrm{IPI} - t_{abs}\right)/\tau_i\right)\right]}.$$

Table 1: Refractory function parameter estimates for strongest-adapting model variants (fits in Fig. 12).

Model	A_1	A_2	t_{abs} (ms)	τ_1 (µs)	τ_2 (ms)	R^2
HH	2.05	1.05	0.329	4.90	0.46	0.935
+HCN(r,3)	1.81	1.21	0.353	3.41	0.35	0.927
+HCN(q,s,4)	1.94	1.17	0.357	2.10	0.42	0.971
+KLT	1.40	1.64	0.360	2.71	0.64	0.969
+HCN(r,3)+KLT	1.74	1.28	0.407	1.79	0.58	0.991
+HCN(q,s,4)+KLT	1.75	1.31	0.403	1.98	0.60	0.995

Absolute refractory period

Figure 13: Absolute refractory period vs. the HCN $V_{1/2}$ shift parameter c for each of the membrane models.

IV. CONCLUSIONS

- Heterogeneity in the half-maximal activation potential of HCN channels can explain the variability of adaptation in SGNs responding to pulsatile CI stimulation while maintaining a physiologically-realistic absolute refractory period.
- HCN channels may be responsible for strong adaptation in response to pulsatile stimulation through the combination of both *spike rate adaptation* and the buildup of *accommodation*.
- The time course over which adaptation acts (8.5–11 ms) qualitatively agrees with the mean rapid adaptation time constant values in cat SGNs (8.2–11.8 ms) (Zhang et al., 2007).
- The +HCN(q,s) model has the largest range in PRRR which is similar to the results found by Miller et al. (2011) and the HCN(q,s) channel model is representative of channels found in the SGN (Liu et al., 2014).

References

Arora, K., Dawson, P., Dowell, R., and Vandali, A. (2009). Electrical stimulation rate effects on speech perception in cochlear implants. *Int J Audiol*, 48(8):561–567.

Chen, G. (1997). Hyperpolarization-activated current (I_h) in primary auditory neurons. *Hear Res*, 110(1-2):179–190.

Heffer, L. F., Sly, D. J., Fallon, J. B., White, M. W., Shepherd, R. K., and O'Leary, S. J. (2010). Examining the auditory nerve fiber response to high rate cochlear implant stimulation: chronic sensorineural hearing loss and facilitation. *J Neurophysiol*, 104(6):3124–3135.

Hugenard, J. R. and McCormick, D. A. (1992). Simulation of the currents involved in rhythmic oscillations in thalamic relay neurons. *J Neurophysiol*, 68(4):1373–1383.

Kim, Y.-H. and Holt, J. R. (2013). Functional contributions of HCN channels in the primary auditory neurons of the mouse inner ear. *The Journal of General Physiology*, 142(3):207–223.

Litvak, L. M., Smith, Z. M., Delgutte, B., and Eddington, D. K. (2003). Desynchronization of electrically evoked auditory-nerve activity by high-frequency pulse trains of long duration. *J Acoust Soc Am*, 114(4 Pt 1):2066–2078.

Liu, Q., Manis, P. B., and Davis, R. L. (2014). I_h and HCN channels in murine spiral ganglion neurons: tonotopic variation, local heterogeneity, and kinetic model. *J Assoc Res Otolaryngol*, 15(4):585–599.

Miller, C. A., Abbas, P. J., and Robinson, B. (2001). Response properties of the refractory auditory nerve fiber. *J Assoc Res Otolaryngol*, 2(3):216–232.

Miller, C. A., Woo, J., Abbas, P. J., Hu, N., and Robinson, B. K. (2011). Neural masking by sub-threshold electric stimuli: animal and computer model results. *J Assoc Res Otolaryngol*, 12(2):219–232.

Mino, H., Rubinstein, J. T., and White, J. A. (2002). Comparison of algorithms for the simulation of action potentials with stochastic sodium channels. *Ann Biomed Eng*, 30(4):578–587.

Mo, Z. L. and Davis, R. L. (1997). Heterogeneous voltage dependence of inward rectifier currents in spiral ganglion neurons. *J Neurophysiol*, 78(6):3019–3027.

Negm, M. H. and Bruce, I. C. (2014). The effects of HCN and KLT ion channels on adaptation and refractoriness in a stochastic auditory nerve model. *IEEE Trans Biomed Eng*, 61(11):2749–2759.

Rothman, J. S. and Manis, P. B. (2003a). Kinetic analyses of three distinct potassium conductances in ventral cochlear nucleus neurons. *J Neurophysiol*, 89(6):3083–3096.

Rothman, J. S. and Manis, P. B. (2003b). The roles potassium currents play in regulating the electrical activity of ventral cochlear nucleus neurons. *J Neurophysiol*, 89(6):3097–3113.

Woo, J., Miller, C. A., and Abbas, P. J. (2009a). Biophysical model of an auditory nerve fiber with a novel adaptation component. *IEEE Trans Biomed Eng*, 56(9):2177–2180.

Woo, J., Miller, C. A., and Abbas, P. J. (2009b). Simulation of the electrically stimulated cochlear neuron: modeling adaptation to trains of electric pulses. *IEEE Trans Biomed Eng*, 56(5):1348–1359.

Woo, J., Miller, C. A., and Abbas, P. J. (2010). The dependence of auditory nerve rate adaptation on electric stimulus parameters, electrode position, and fiber diameter: a computer model study. *J Assoc Res Otolaryngol*, 11(2):283–296.

Yi, E., Roux, I., and Glowatzki, E. (2010). Dendritic HCN channels shape excitatory postsynaptic potentials at the inner hair cell afferent synapse in the mammalian cochlea. *J Neurophysiol*, 103(5):2532–2543.

Zhang, F., Miller, C. A., Robinson, B. K., Abbas, P. J., and Hu, N. (2007). Changes across time in spike rate and spike amplitude of auditory nerve fibers stimulated by electric pulse trains. *J Assoc Res Otolaryngol*, 8(3):356–372.

jason.boulet@gmail.com | ibruce@ieee.org